

# Structural modal reanalysis using automated matrix permutation and substructuring

Seung-Hwan Boo\*

Division of Naval Architecture and Ocean Systems Engineering, Korea Maritime and Ocean University,  
727 Taejong-ro, Yeongdo-gu, Busan 49112, Republic of Korea

(Received October 24, 2018, Revised November 22, 2018, Accepted November 23, 2018)

**Abstract.** In this paper, a new efficient method for structural modal reanalysis is proposed, which can handle large finite element (FE) models requiring frequent design modifications. The global FE model is divided into a residual part not to be modified and a target part to be modified. Then, an automated matrix permutation and substructuring algorithm is applied to these parts independently. The reduced model for the residual part is calculated and saved in the initial analysis, and the target part is reduced repeatedly, whenever design modifications occur. Then, the reduced model for the target part is assembled with that of the residual part already saved; thus, the final reduced model corresponding to the new design is obtained easily and rapidly. Here, the formulation of the proposed method is derived in detail, and its computational efficiency and reanalysis ability are demonstrated through several engineering problems, including a topological modification.

**Keywords:** structural modal reanalysis; finite element method; model reduction; substructuring; eigenvalue problem

## 1. Introduction

Over recent decades, computer performance has improved significantly, and this allows us to simulate larger and more complex structures by modeling with finite elements (FE). However, despite this improvement, structural modal analysis of large FE models that requires solving eigenvalue problems is still a time-consuming task. Furthermore, considering the fact that design modifications generally occur several times until design completion, it is highly inefficient to perform structural modal analysis repeatedly at each design change. Therefore, to resolve this computational burden, it is attractive to employ model reduction methods, such as component mode synthesis (CMS) (Craig and Bampton 1968, Benfield and Hruda 1971, Rubin 1975, Papadimiriou and Papadioti 2013).

For CMS, a global FE model is divided into several substructural models to construct a reduced model more efficiently. For this reason, CMS methods have been often referred to as a substructuring technique. In structural modal reanalysis using CMS methods (Chen and Rong 2002, Perdahcioğlu *et al.* 2011, Kaveh and Faxli 2011, Jian-Jun *et al.* 2015), the key feature of the substructuring technique (all computations are accomplished based on the substructures) is utilized effectively. If design modifications affecting such as thickness, materials, or mesh changes occur in particular substructures, the substructural normal modes and constraint modes corresponding to those substructures are computed newly, and then only the new results are used to update the previous reduced model.

Therefore, much of the computation time needed to construct a reduced model for the new design can be saved.

However, CMS methods are based on domain-based substructuring (Leung 1979, Soize and Mziou 2003, Han 2014), in which the substructuring process is performed considering geometrical characteristics of the structure. Therefore, if a large FE model is considered, it is not easy to make such a large number of substructures, and the substructures must contain relatively large degrees of freedom (DOFs). Thus, huge computational costs are required for the eigenvalue analysis and for the inverse process of the stiffness matrix for substructures (Boo and Oh 2017, Boo *et al.* 2018).

Recalling that the main purpose for employing the substructuring technique is to compute the reduced model efficiently, domain-based substructuring has the limitation to deal with larger, more complicated FE models involving several millions of DOFs.

To address this limitation, the automated substructuring algorithm (George 1973, Hendrickson and Rothberg 1997, Karypis and Kumar 1998) was developed. In the automated substructuring algorithm, the global matrix is appropriately permuted, and the permuted matrix is automatically partitioned into hundreds of submatrices (substructures) from the algebraic perspective. Automated substructuring has been applied successfully to CMS methods, and several robust methods, such as the automated multi-level substructuring (AMLS) method (Kaplan 2001, Bennighof and Lehoucq 2004), algebraic dynamic condensation (ADC) method (Boo and Lee 2017), and iterative algebraic dynamic condensation (IADC) method (Boo and Lee 2017) have been developed. These methods allow handling of FE models with more than a million DOFs with remarkable computational efficiency.

In this paper, a new, more efficient structural modal

---

\*Corresponding author, Professor  
E-mail: shboo@kmou.ac.kr

reanalysis method is proposed employing the automated matrix permutation and substructuring. First, a global FE model is divided into a residual part not to be modified and a target part to be modified. The automated matrix permutation and substructuring algorithm is applied to these parts, and each reduced model is calculated using the AMLS method. The reduced model for the residual part, including most of the total DOFs, is saved in the initial analysis, and is reused in each structural modal reanalysis.

On the other hand, the reduced model for the target part is calculated repeatedly, whenever design modifications are considered. Because the reduced model for the target part is assembled with that of the residual part already saved, the final reduced model corresponding to the new design can be obtained easily and quickly. This is the most significant feature for reducing computation times with the proposed structural modal reanalysis method.

In the following sections, the general structural modal reanalysis procedure for handling the global FE models is briefly demonstrated, and the formulation of the proposed method is derived in detail with a form of submatrix computation. Then, the computational efficiency and reanalysis ability of the proposed method are demonstrated through several large engineering FE models.

## 2. Structural modal reanalysis for global FE models

The structural modal analysis for an initial global FE model is conducted using the following generalized eigenvalue problem

$$\mathbf{K}\boldsymbol{\phi} = \lambda\mathbf{M}\boldsymbol{\phi} \quad (1)$$

where  $\mathbf{M}$  and  $\mathbf{K}$  denote the initial global mass and stiffness matrices, respectively, and  $\boldsymbol{\phi}$  and  $\lambda$  denote the eigenvector and eigenvalue of the initial global structure, respectively.

Considering design modifications without increasing the DOFs, the following updated global mass and stiffness matrices are obtained.

$$\tilde{\mathbf{M}} = \mathbf{M} + \Delta\mathbf{M}, \quad \tilde{\mathbf{K}} = \mathbf{K} + \Delta\mathbf{K} \quad (2)$$

in which  $\Delta\mathbf{M}$  and  $\Delta\mathbf{K}$  are the added mass and stiffness matrices resulting from the design modifications considered, and the notation  $\sim$  represents the updated terms.

Thus, the generalized eigenvalue problem for the modified global FE model can be defined as

$$\tilde{\mathbf{K}}\tilde{\boldsymbol{\phi}} = \tilde{\lambda}\tilde{\mathbf{M}}\tilde{\boldsymbol{\phi}} \quad (3)$$

where  $\tilde{\boldsymbol{\phi}}$  and  $\tilde{\lambda}$  denote the eigenvector and eigenvalue of the modified global structure, respectively.

However, when solving large FE models containing several hundreds of thousands of DOFs, the generalized eigenvalue problems in Eq. (1) and Eq. (3) require huge computation times and computer resources. Furthermore, considering that design modifications would be reflected several times during the stages of design, it would be highly inefficient to compute the eigenpairs of such large FE models repeatedly at each new stage of design. To handle

this inefficiency, a new structural modal reanalysis method is proposed in this paper.

## 3. New structural modal reanalysis method

In this section, a new structural modal reanalysis method is described. The key processes of the proposed method are: (1) Definition of the residual and target parts, (2) Automated matrix permutation and substructuring, (3) Reduction of the target and residual parts, (4) Assemblage of the reduced matrices and solving the reduced system.

### 3.1 Definition of the residual and target parts

Let us consider a global FE model requiring design modifications, as shown in Fig. 1(a). The global structure is divided into three parts:  $\Omega_a$ ,  $\Omega_b$ , and  $\Omega_\Gamma$ . Here,  $\Omega_\Gamma$  denotes the interface boundary between  $\Omega_a$  and  $\Omega_b$ , and  $\Omega_\Gamma$  can be divided into  $\Omega_\alpha$  and  $\Omega_\beta$ , as shown in Fig. 1(b). This means that  $\Omega_\Gamma = \Omega_\alpha \cup \Omega_\beta$ .

Thus, the global FE model can be partitioned into two parts,  $\Omega_A$  and  $\Omega_B$ , as shown in Fig. 1(b). Here,  $\Omega_A$  denotes the “residual” part that would not be modified, and  $\Omega_B$  denotes the “target” part that would be modified due to design modifications affecting such as thickness, materials, or mesh changes.

The target part  $\Omega_B$  is divided into updating and intermediate regions, as shown in Fig. 1(c). The intermediate region would not be changed to avoid unnecessary updating at the interface boundary  $\Omega_\beta$ . The updating region is indicated with a blue color, and after reflecting design modifications in the updating region, the target part  $\Omega_B$  would be updated to  $\hat{\Omega}_B$ .

Based on Fig. 1(a), the mass and stiffness matrices for the initial global FE model are expressed as

$$\mathbf{M} = \begin{bmatrix} \mathbf{M}_a & \mathbf{M}_{a,\Gamma} & \mathbf{0} \\ \mathbf{M}_{a,\Gamma}^T & \mathbf{M}_\Gamma & \mathbf{M}_{\Gamma,b} \\ \mathbf{0} & \mathbf{M}_{\Gamma,b}^T & \mathbf{M}_b \end{bmatrix}, \quad \mathbf{K} = \begin{bmatrix} \mathbf{K}_a & \mathbf{K}_{a,\Gamma} & \mathbf{0} \\ \mathbf{K}_{a,\Gamma}^T & \mathbf{K}_\Gamma & \mathbf{K}_{\Gamma,b} \\ \mathbf{0} & \mathbf{K}_{\Gamma,b}^T & \mathbf{K}_b \end{bmatrix} \quad (4)$$

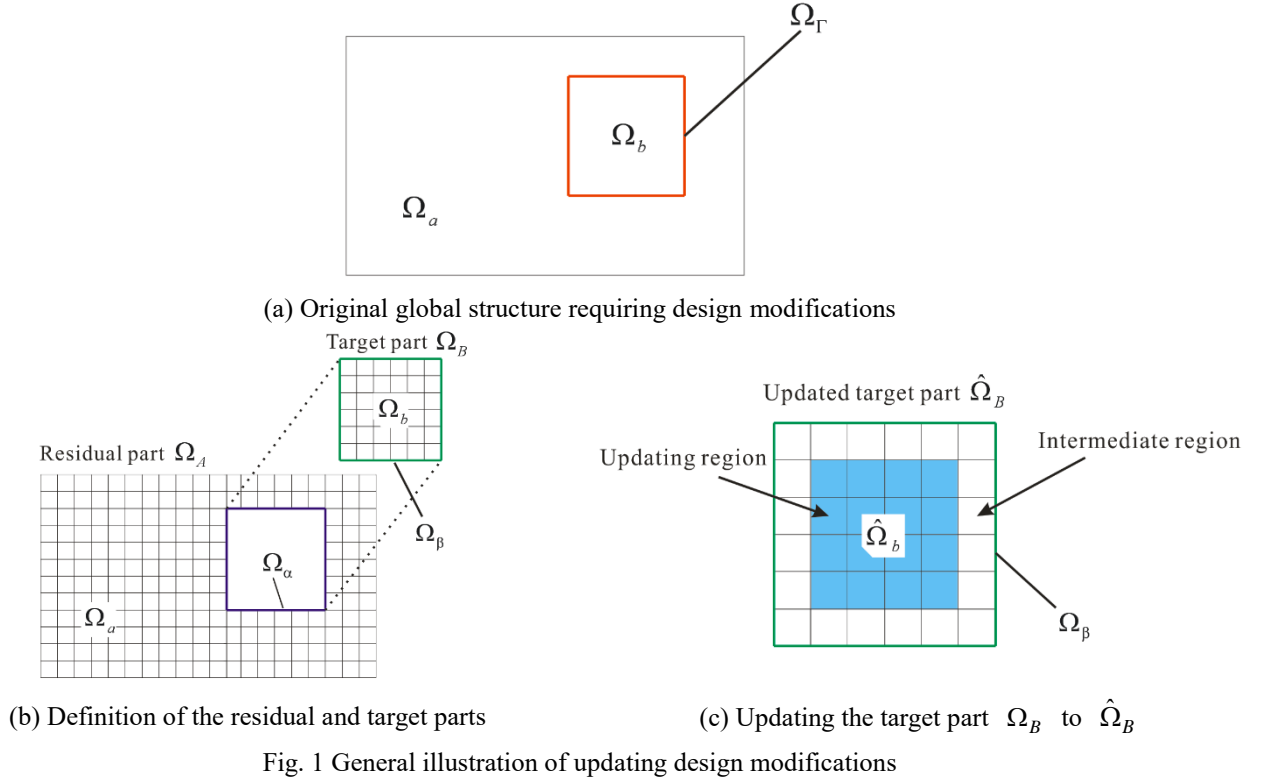
where the subscripts  $a$  and  $b$  denote the quantities corresponding to  $\Omega_a$  and  $\Omega_b$ , and  $\Gamma$  denotes the quantity corresponding to the interface boundary  $\Omega_\Gamma$ .

The matrices  $\mathbf{M}_\Gamma$  and  $\mathbf{K}_\Gamma$  in Eq. (4), corresponding to the interface boundary  $\Omega_\Gamma$ , can be divided into parts as follows

$$\mathbf{M}_\Gamma = \mathbf{M}_\alpha + \mathbf{M}_\beta, \quad \mathbf{K}_\Gamma = \mathbf{K}_\alpha + \mathbf{K}_\beta \quad (5)$$

in which the subscripts  $\alpha$  and  $\beta$  represent the quantities corresponding to  $\Omega_\alpha$  and  $\Omega_\beta$ , respectively.

From Eq. (5) and Fig. 1(b), the initial global mass and stiffness matrices  $\mathbf{M}$  and  $\mathbf{K}$  in Eq. (4) can be partitioned



as follows

$$\mathbf{M}_A = \begin{bmatrix} \mathbf{M}_a & \mathbf{M}_{a,\Gamma} \\ \mathbf{M}_{a,\Gamma}^T & \mathbf{M}_\alpha \end{bmatrix}, \quad \mathbf{M}_B = \begin{bmatrix} \mathbf{M}_\beta & \mathbf{M}_{\Gamma,b} \\ \mathbf{M}_{\Gamma,b}^T & \mathbf{M}_b \end{bmatrix} \quad (6)$$

$$\mathbf{K}_A = \begin{bmatrix} \mathbf{K}_a & \mathbf{K}_{a,\Gamma} \\ \mathbf{K}_{a,\Gamma}^T & \mathbf{K}_\alpha \end{bmatrix}, \quad \mathbf{K}_B = \begin{bmatrix} \mathbf{K}_\beta & \mathbf{K}_{\Gamma,b} \\ \mathbf{K}_{\Gamma,b}^T & \mathbf{K}_b \end{bmatrix}$$

where  $\mathbf{M}_A$  and  $\mathbf{K}_A$  are the mass and stiffness matrices corresponding to the residual part  $\Omega_A$ , and  $\mathbf{M}_B$  and  $\mathbf{K}_B$  are the mass and stiffness matrices corresponding to the target part  $\Omega_B$ .

After reflecting design modifications, the mass and stiffness matrices  $\mathbf{M}_B$  and  $\mathbf{K}_B$  (corresponding to the target part  $\Omega_B$ ) are updated as follows

$$\tilde{\mathbf{M}}_B = \begin{bmatrix} \mathbf{M}_\beta & \tilde{\mathbf{M}}_{\Gamma,b} \\ \tilde{\mathbf{M}}_{\Gamma,b}^T & \tilde{\mathbf{M}}_b \end{bmatrix}, \quad \tilde{\mathbf{K}}_B = \begin{bmatrix} \mathbf{K}_\beta & \tilde{\mathbf{K}}_{\Gamma,b} \\ \tilde{\mathbf{K}}_{\Gamma,b}^T & \tilde{\mathbf{K}}_b \end{bmatrix}. \quad (7)$$

Note that the matrices corresponding to the residual part  $\Omega_A$  ( $\mathbf{M}_A$  and  $\mathbf{K}_A$ ) would not be changed by the design modifications considered.

### 3.2 Automated matrix permutation and substructuring

The automated matrix permutation and substructuring algorithm (Karypis and Kumar 1998) gives a permutation vector  $\mathbf{P}$ , and using this vector, an arbitrary sparse matrix  $\mathbf{A}$  is permuted as follows

$$\mathbf{A}_p = \mathbf{A}(\mathbf{P}, \mathbf{P}) \quad (8)$$

where  $\mathbf{A}_p$  denotes the permuted sparse matrix. The matrix permutation is equivalent to the renumbering of nodes in FE models. Therefore, the physical characteristic of the original FE model is not changed.

After the permutation, the matrix  $\mathbf{A}_p$  is divided into many submatrices. Then, those submatrices are designated as substructures in the algebraic perspective, and the substructural leveling graph, which defines the relationships among the substructures, is constructed. For better understanding, the details are drawn in Fig. 2.

In the proposed method, the automated matrix permutation and substructuring algorithm is applied to the residual part  $\Omega_A$  and to the target part  $\Omega_B$ , individually. Thus, the permutation vectors  $\mathbf{P}_A$  and  $\mathbf{P}_B$  (corresponding to  $\Omega_A$  and  $\Omega_B$ ) are derived.

The permutation vectors  $\mathbf{P}_A$  and  $\mathbf{P}_B$  are rearranged beforehand to prepare the matrix assemblage for  $\Omega_A$  and  $\Omega_B$  as follows, which is the last process of the proposed method.

$$\mathbf{P}'_A = \begin{bmatrix} \mathbf{P}_a \\ \mathbf{P}_\alpha \end{bmatrix}, \quad \mathbf{P}'_B = \begin{bmatrix} \mathbf{P}_\beta \\ \mathbf{P}_b \end{bmatrix} \quad (9)$$

where  $\mathbf{P}'_A$  and  $\mathbf{P}'_B$  are the rearranged vectors for  $\mathbf{P}_A$  and  $\mathbf{P}_B$ , respectively, and  $\mathbf{P}_a$ ,  $\mathbf{P}_b$ ,  $\mathbf{P}_\alpha$ , and  $\mathbf{P}_\beta$  are the vectors corresponding to  $\Omega_a$ ,  $\Omega_b$ ,  $\Omega_\alpha$ , and  $\Omega_\beta$  in the

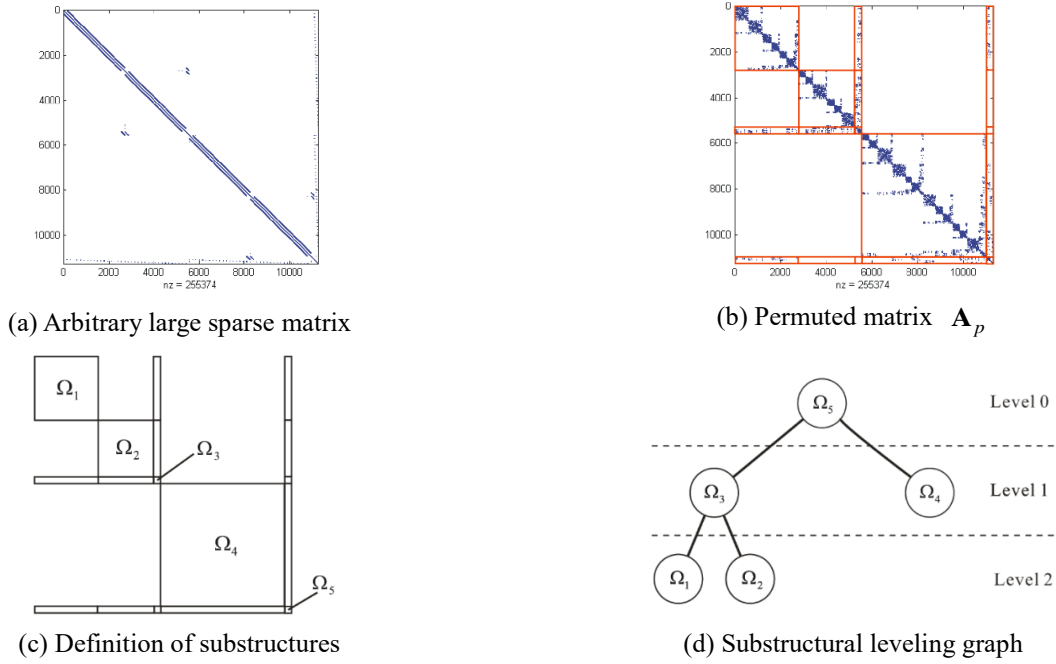


Fig. 2 Automated matrix permutation and substructuring

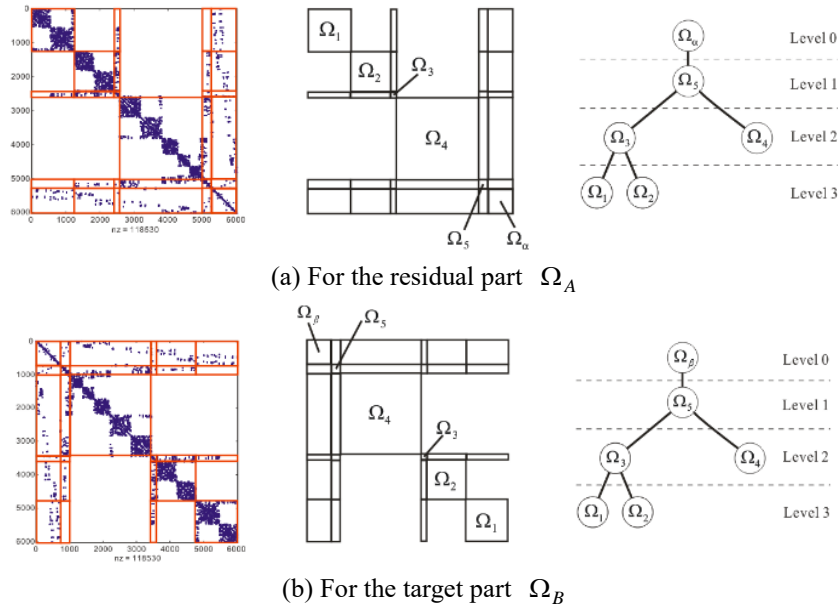


Fig. 3 Automated matrix permutation and substructuring in the proposed method

permutation vectors  $\mathbf{P}_A$  and  $\mathbf{P}_B$ . This rearrange is conducted easily by considering the node numbers of  $\Omega_a$ ,  $\Omega_b$ ,  $\Omega_\alpha$ , and  $\Omega_\beta$ .

From Eq. (8) and Eq. (9), the permuted mass and stiffness matrices for  $\Omega_A$  and  $\Omega_B$  are obtained as follows

$$\mathbf{M}_A = \mathbf{M}_A(\mathbf{P}'_A, \mathbf{P}'_A), \quad \mathbf{K}_A = \mathbf{K}_A(\mathbf{P}'_A, \mathbf{P}'_A) \quad (10a)$$

$$\mathbf{M}_B = \mathbf{M}_B(\mathbf{P}'_B, \mathbf{P}'_B), \quad \mathbf{K}_B = \mathbf{K}_B(\mathbf{P}'_B, \mathbf{P}'_B). \quad (10b)$$

Note that, to avoid confusion from the usage of different

matrix notations, the same notation is used for the original and permuted matrices in Eq. (10).

The detailed process of automated matrix permutation and substructuring for  $\Omega_A$  and  $\Omega_B$  are illustrated in Fig. 3. Here, five substructures and the interface boundaries ( $\Omega_\alpha$  and  $\Omega_\beta$ ) are defined with three substructural levels for  $\Omega_A$  and  $\Omega_B$ . Note that the number of substructural levels and substructures depends on the number of DOFs in  $\Omega_A$  and  $\Omega_B$ .

Based on Fig. 3, the matrices  $\mathbf{M}_A$  and  $\mathbf{K}_A$  for the residual part  $\Omega_A (= \Omega_a \cup \Omega_\alpha)$  are represented in



The substructural constraint modes matrix for the 1<sup>st</sup> substructure is defined by

$$\Psi_{1,j} = -\mathbf{K}_1^{-1} \mathbf{K}_{1,j} \quad \text{for } j \in A_1 \quad (14)$$

where  $\Psi_{1,j}$  is the substructural constraint modes matrix between the 1<sup>st</sup> substructure and its ancestor substructures ( $j^{\text{th}}$  substructure).

Using Eq. (13) and Eq. (14), the 1<sup>st</sup> transformation matrix for the target part  $\Omega_B$  is defined by

$$\mathbf{T}_1^B = \begin{bmatrix} \mathbf{I}_\beta & & & & & \\ \mathbf{0} & \mathbf{I}_5 & & & & \mathbf{0} \\ \mathbf{0} & \mathbf{0} & \mathbf{I}_4 & & & \\ \mathbf{0} & \mathbf{0} & \mathbf{0} & \mathbf{I}_3 & & \\ \mathbf{0} & \mathbf{0} & \mathbf{0} & \mathbf{0} & \mathbf{I}_2 & \\ \Psi_{1,\Gamma} & \Psi_{1,5} & \mathbf{0} & \Psi_{1,3} & \mathbf{0} & \Phi_1^d \end{bmatrix} \quad (15)$$

in which  $\mathbf{I}_i$  and  $\mathbf{I}_\beta$  are the identity matrix corresponding to the  $i^{\text{th}}$  substructure and the interface boundary  $\Omega_\beta$ , respectively. The transformation matrices for the target part  $\Omega_B$  are lower triangular matrices.

Using the 1<sup>st</sup> transformation matrix  $\mathbf{T}_1^B$ , the 1<sup>st</sup> transformed mass and stiffness matrices for the target part  $\Omega_B$  are obtained as follows

$$\hat{\mathbf{M}}_B^{(1)} = (\mathbf{T}_1^B)^T \mathbf{M}_B \mathbf{T}_1^B, \quad \hat{\mathbf{K}}_B^{(1)} = (\mathbf{T}_1^B)^T \mathbf{K}_B \mathbf{T}_1^B \quad (16)$$

where the hat  $\hat{\phantom{x}}$  denotes the incompletely transformed term during the transformation procedures.

The 1<sup>st</sup> transformed matrices  $\hat{\mathbf{M}}_B^{(1)}$  and  $\hat{\mathbf{K}}_B^{(1)}$  are represented in a substructural matrix form as follows

$$\hat{\mathbf{M}}_B^{(1)} = \begin{bmatrix} \hat{\mathbf{M}}_\beta^{(1)} & & & & & \\ \hat{\mathbf{M}}_{5,\Gamma}^{(1)} & \hat{\mathbf{M}}_5^{(1)} & & & & \text{sym.} \\ \mathbf{M}_{4,\Gamma} & \mathbf{M}_{4,5} & \mathbf{M}_4 & & & \\ \hat{\mathbf{M}}_{3,\Gamma}^{(1)} & \hat{\mathbf{M}}_{3,5}^{(1)} & \mathbf{0} & \hat{\mathbf{M}}_3^{(1)} & & \\ \mathbf{M}_{2,\Gamma} & \mathbf{M}_{2,5} & \mathbf{0} & \mathbf{M}_{2,3} & \mathbf{M}_2 & \\ \hat{\mathbf{M}}_{1,\Gamma}^{(1)} & \hat{\mathbf{M}}_{1,5}^{(1)} & \mathbf{0} & \hat{\mathbf{M}}_{1,3}^{(1)} & \mathbf{0} & \mathbf{I}_1^d \end{bmatrix} \quad (17)$$

$$\hat{\mathbf{K}}_B^{(1)} = \begin{bmatrix} \hat{\mathbf{K}}_\beta^{(1)} & & & & & \\ \hat{\mathbf{K}}_{5,\Gamma}^{(1)} & \hat{\mathbf{K}}_5^{(1)} & & & & \text{sym.} \\ \mathbf{K}_{4,\Gamma} & \mathbf{K}_{4,5} & \mathbf{K}_4 & & & \\ \hat{\mathbf{K}}_{3,\Gamma}^{(1)} & \hat{\mathbf{K}}_{3,5}^{(1)} & \mathbf{0} & \hat{\mathbf{K}}_3^{(1)} & & \\ \mathbf{K}_{2,\Gamma} & \mathbf{K}_{2,5} & \mathbf{0} & \mathbf{K}_{2,3} & \mathbf{K}_2 & \\ \mathbf{0} & \mathbf{0} & \mathbf{0} & \mathbf{0} & \mathbf{0} & \Lambda_1^d \end{bmatrix}$$

$$\hat{\mathbf{M}}_{1,j}^{(1)} = (\Phi_1^d)^T (\mathbf{M}_{1,j} + \mathbf{M}_1 \Psi_{1,j}) \quad \text{for } j \in A_1 \quad (18a)$$

$$\hat{\mathbf{M}}_{i,j}^{(1)} = \mathbf{M}_{i,j} + \Psi_{1,i}^T \mathbf{M}_{1,j} + \mathbf{M}_{1,i}^T \Psi_{1,j} + \Psi_{1,i}^T \mathbf{M}_1 \Psi_{1,j} \quad (18b)$$

for  $i, j \in A_1$

$$\hat{\mathbf{K}}_{i,j}^{(1)} = \mathbf{K}_{i,j} + \Psi_{1,i}^T \mathbf{K}_{1,j} \quad \text{for } i, j \in A_1 \quad (18c)$$

$$\mathbf{I}_1^d = (\Phi_1^d)^T \mathbf{M}_1 (\Phi_1^d), \quad \Lambda_1^d = (\Phi_1^d)^T \mathbf{K}_1 (\Phi_1^d) \quad (18d)$$

Note that, in the mass matrix  $\hat{\mathbf{M}}_B^{(1)}$ , the substructural matrices related to the 1<sup>st</sup> substructure and its ancestor substructures ( $\in A_1$ ) are only updated by  $\mathbf{T}_1^B$ . For the stiffness matrix  $\hat{\mathbf{K}}_B^{(1)}$ , the updating characteristic is similar to that of  $\hat{\mathbf{M}}_B^{(1)}$ , except that the off-diagonal substructural matrices in the 1<sup>st</sup> row become zero matrices.

In the same way, the 2<sup>nd</sup> transformation matrix  $\mathbf{T}_2^B$  can be computed, and the 2<sup>nd</sup> transformed mass and stiffness matrices for the target part  $\Omega_B$  are obtained as

$$\hat{\mathbf{M}}_B^{(2)} = (\mathbf{T}_2^B)^T \hat{\mathbf{M}}_B^{(1)} \mathbf{T}_2^B, \quad \hat{\mathbf{K}}_B^{(2)} = (\mathbf{T}_2^B)^T \hat{\mathbf{K}}_B^{(1)} \mathbf{T}_2^B. \quad (19)$$

After the transformation procedures for the bottom substructures ( $\in B$ ), the transformation procedures for the higher substructures ( $\in H$ ) are accomplished. For the 3<sup>rd</sup> substructure, the higher substructure belonging to the 2<sup>nd</sup> substructural level, the substructural eigenvalue problem is given by

$$\hat{\mathbf{K}}_3^{(2)} \Phi_3 = \hat{\mathbf{M}}_3^{(2)} \Phi_3 \Lambda_3$$

$$\text{with } \Phi_3 = [\Phi_3^d \quad \Phi_3^t], \quad \Lambda_3 = \begin{bmatrix} \Lambda_3^d & \mathbf{0} \\ \mathbf{0} & \Lambda_3^t \end{bmatrix} \quad (20)$$

and the substructural constraint modes matrix for the 3<sup>rd</sup> substructure is calculated by

$$\Psi_{3,j} = -(\hat{\mathbf{K}}_3^{(2)})^{-1} \hat{\mathbf{K}}_{3,j}^{(2)} \quad \text{for } j \in A_3 \quad (21)$$

where  $\hat{\mathbf{M}}_3^{(2)}$  and  $\hat{\mathbf{K}}_3^{(2)}$  are the substructural mass and stiffness matrix corresponding to the 3<sup>rd</sup> substructure in  $\hat{\mathbf{M}}_B^{(2)}$  and  $\hat{\mathbf{K}}_B^{(2)}$  in Eq. (19). The matrix  $\hat{\mathbf{K}}_{3,j}^{(2)}$  denotes the off-diagonal component matrix to couple the 3<sup>rd</sup> substructure and its ancestor substructures in  $\hat{\mathbf{K}}_B^{(2)}$ .

Using Eq. (20) and Eq. (21), the 3<sup>rd</sup> transformation matrix  $\mathbf{T}_3^B$  is obtained by

$$\mathbf{T}_3^B = \begin{bmatrix} \mathbf{I}_\beta & & & & & \\ \mathbf{0} & \mathbf{I}_5 & & & & \mathbf{0} \\ \mathbf{0} & \mathbf{0} & \mathbf{I}_4 & & & \\ \Psi_{3,\Gamma} & \Psi_{3,5} & \mathbf{0} & \Phi_3^d & & \\ \mathbf{0} & \mathbf{0} & \mathbf{0} & \mathbf{0} & \mathbf{I}_2^d & \\ \mathbf{0} & \mathbf{0} & \mathbf{0} & \mathbf{0} & \mathbf{0} & \mathbf{I}_1^d \end{bmatrix} \quad (22)$$

and then, the 3<sup>rd</sup> transformed mass and stiffness matrices for the target part  $\Omega_B$  are obtained by

$$\hat{\mathbf{M}}_B^{(3)} = (\mathbf{T}_3^B)^T \hat{\mathbf{M}}_B^{(2)} \mathbf{T}_3^B, \quad \hat{\mathbf{K}}_B^{(3)} = (\mathbf{T}_3^B)^T \hat{\mathbf{K}}_B^{(2)} \mathbf{T}_3^B. \quad (23)$$

The detailed formulations for  $\hat{\mathbf{M}}_B^{(3)}$  and  $\hat{\mathbf{K}}_B^{(3)}$  are

represented as

$$\hat{\mathbf{M}}_B^{(3)} = \begin{bmatrix} \hat{\mathbf{M}}_\beta^{(3)} & & & & & \\ \hat{\mathbf{M}}_{5,\Gamma}^{(3)} & \hat{\mathbf{M}}_5^{(3)} & & & & \text{sym.} \\ \hat{\mathbf{M}}_{4,\Gamma}^{(3)} & \hat{\mathbf{M}}_{4,5}^{(3)} & \hat{\mathbf{M}}_4^{(3)} & & & \\ \hat{\mathbf{M}}_{3,\Gamma}^{(3)} & \hat{\mathbf{M}}_{3,5}^{(3)} & \mathbf{0} & \mathbf{I}_3^d & & \\ \hat{\mathbf{M}}_{2,\Gamma}^{(3)} & \hat{\mathbf{M}}_{2,5}^{(3)} & \mathbf{0} & \bar{\mathbf{M}}_{2,3} & \mathbf{I}_2^d & \\ \hat{\mathbf{M}}_{1,\Gamma}^{(3)} & \hat{\mathbf{M}}_{1,5}^{(3)} & \mathbf{0} & \bar{\mathbf{M}}_{1,3} & \mathbf{0} & \mathbf{I}_1^d \end{bmatrix} \quad (24)$$

$$\hat{\mathbf{K}}_B^{(3)} = \begin{bmatrix} \hat{\mathbf{K}}_\beta^{(3)} & & & & & \\ \hat{\mathbf{K}}_{5,\Gamma}^{(3)} & \hat{\mathbf{K}}_5^{(3)} & & & & \text{sym.} \\ \hat{\mathbf{K}}_{4,\Gamma}^{(3)} & \hat{\mathbf{K}}_{4,5}^{(3)} & \hat{\mathbf{K}}_4^{(3)} & & & \\ \mathbf{0} & \mathbf{0} & \mathbf{0} & \Lambda_3^d & & \\ \mathbf{0} & \mathbf{0} & \mathbf{0} & \mathbf{0} & \Lambda_2^d & \\ \mathbf{0} & \mathbf{0} & \mathbf{0} & \mathbf{0} & \mathbf{0} & \Lambda_1^d \end{bmatrix} \quad (25a)$$

$$\bar{\mathbf{M}}_{i,3} = \bar{\mathbf{M}}_{i,3}^{(2)} \Phi_3^d \text{ for } i \in C_3 \quad (25a)$$

$$\hat{\mathbf{M}}_{3,j}^{(3)} = (\Phi_3^d)^T (\hat{\mathbf{M}}_{3,j}^{(2)} + \hat{\mathbf{M}}_3^{(2)} \Psi_{3,j}) \text{ for } j \in A_3 \quad (25b)$$

$$\hat{\mathbf{M}}_{i,j}^{(3)} = \hat{\mathbf{M}}_{i,j}^{(2)} + \hat{\mathbf{M}}_{i,3}^{(2)} \Psi_{3,j} \text{ for } i \in C_3 \text{ and } j \in A_3 \quad (25c)$$

$$\hat{\mathbf{M}}_{i,j}^{(3)} = \hat{\mathbf{M}}_{i,j}^{(2)} + \Psi_{3,i}^T \hat{\mathbf{M}}_{3,j}^{(2)} + (\hat{\mathbf{M}}_{3,i}^{(2)})^T \Psi_{3,j} + \Psi_{3,i}^T \hat{\mathbf{M}}_3^{(2)} \Psi_{3,j} \quad (25d)$$

for  $i, j \in A_3$

$$\hat{\mathbf{K}}_{i,j}^{(3)} = \hat{\mathbf{K}}_{i,j}^{(2)} + \Psi_{3,i}^T \hat{\mathbf{K}}_{3,j}^{(2)} \text{ for } i, j \in A_3 \quad (25e)$$

$$\mathbf{I}_3^d = (\Phi_3^d)^T \hat{\mathbf{M}}_3^{(2)} (\Phi_3^d), \quad \Lambda_3^d = (\Phi_3^d)^T \hat{\mathbf{K}}_3^{(2)} (\Phi_3^d). \quad (25f)$$

In the same way, the transformation matrices  $\mathbf{T}_4^B$  and  $\mathbf{T}_5^B$ , corresponding to the remaining higher substructures ( $\in H$ ), can be computed. After conducting the transformation procedures with  $\mathbf{T}_4^B$  and  $\mathbf{T}_5^B$  sequentially, the completely transformed reduced mass and stiffness matrices for the target part,  $\bar{\mathbf{M}}_B$  and  $\bar{\mathbf{K}}_B$ , are obtained as follows

$$\bar{\mathbf{M}}_B = (\mathbf{T}_5^B)^T \hat{\mathbf{M}}_B^{(4)} \mathbf{T}_5^B, \quad \bar{\mathbf{K}}_B = (\mathbf{T}_5^B)^T \hat{\mathbf{K}}_B^{(4)} \mathbf{T}_5^B, \quad (26)$$

$$\text{with } \hat{\mathbf{M}}_B^{(4)} = (\mathbf{T}_4^B)^T \hat{\mathbf{M}}_B^{(3)} \mathbf{T}_4^B, \quad \hat{\mathbf{K}}_B^{(4)} = (\mathbf{T}_4^B)^T \hat{\mathbf{K}}_B^{(3)} \mathbf{T}_4^B.$$

The detailed formulations of the final reduced mass and stiffness matrices for the target part  $\Omega_B$ ,  $\bar{\mathbf{M}}_B$  and  $\bar{\mathbf{K}}_B$ , are expressed as

$$\bar{\mathbf{M}}_B = \begin{bmatrix} \hat{\mathbf{M}}_\beta^{(5)} & & & & & \\ \hat{\mathbf{M}}_{5,\Gamma}^{(5)} & \mathbf{I}_5^d & & & & \\ \hat{\mathbf{M}}_{4,\Gamma}^{(5)} & \bar{\mathbf{M}}_{4,5} & \mathbf{I}_4^d & & & \text{sym.} \\ \hat{\mathbf{M}}_{3,\Gamma}^{(5)} & \bar{\mathbf{M}}_{3,5} & \mathbf{0} & \mathbf{I}_3^d & & \\ \hat{\mathbf{M}}_{2,\Gamma}^{(5)} & \bar{\mathbf{M}}_{2,5} & \mathbf{0} & \bar{\mathbf{M}}_{2,3} & \mathbf{I}_2^d & \\ \hat{\mathbf{M}}_{1,\Gamma}^{(5)} & \bar{\mathbf{M}}_{1,5} & \mathbf{0} & \bar{\mathbf{M}}_{1,3} & \mathbf{0} & \mathbf{I}_1^d \end{bmatrix} \quad (27)$$

$$\bar{\mathbf{K}}_B = \begin{bmatrix} \hat{\mathbf{K}}_\beta^{(5)} & & & & & \\ \mathbf{0} & \Lambda_5^d & & & & \\ \mathbf{0} & \mathbf{0} & \Lambda_4^d & & & \text{sym.} \\ \mathbf{0} & \mathbf{0} & \mathbf{0} & \Lambda_3^d & & \\ \mathbf{0} & \mathbf{0} & \mathbf{0} & \mathbf{0} & \Lambda_2^d & \\ \mathbf{0} & \mathbf{0} & \mathbf{0} & \mathbf{0} & \mathbf{0} & \Lambda_1^d \end{bmatrix}$$

$$\bar{\mathbf{M}}_{i,5} = \hat{\mathbf{M}}_{i,5}^{(4)} \Phi_5^d \text{ for } i \in C_5 \quad (28a)$$

$$\hat{\mathbf{M}}_{5,\Gamma}^{(5)} = (\Phi_5^d)^T (\hat{\mathbf{M}}_{5,\Gamma}^{(4)} + \hat{\mathbf{M}}_5^{(4)} \Psi_{5,\Gamma}) \quad (28b)$$

$$\hat{\mathbf{M}}_{i,\Gamma}^{(5)} = \hat{\mathbf{M}}_{i,\Gamma}^{(4)} + \hat{\mathbf{M}}_{i,5}^{(4)} \Psi_{5,\Gamma} \text{ for } i \in C_5 \quad (28c)$$

$$\hat{\mathbf{M}}_\beta^{(5)} = \hat{\mathbf{M}}_\beta^{(4)} + \Psi_{5,\beta}^T \hat{\mathbf{M}}_{5,\beta}^{(4)} + (\hat{\mathbf{M}}_{5,\beta}^{(4)})^T \Psi_{5,\beta} + \Psi_{5,\beta}^T \hat{\mathbf{M}}_5^{(4)} \Psi_{5,\beta} \quad (28d)$$

$$\hat{\mathbf{K}}_\beta^{(5)} = \hat{\mathbf{K}}_\beta^{(4)} + \Psi_{5,\beta}^T \hat{\mathbf{K}}_{5,\beta}^{(4)} \quad (28e)$$

$$\mathbf{I}_5^d = (\Phi_5^d)^T \hat{\mathbf{M}}_5^{(4)} (\Phi_5^d), \quad \Lambda_5^d = (\Phi_5^d)^T \hat{\mathbf{K}}_5^{(4)} (\Phi_5^d). \quad (28f)$$

In the proposed method, the mass and stiffness matrices corresponding to the interface boundary  $\Omega_\beta$  (= the highest substructure),  $\hat{\mathbf{M}}_\beta^{(5)}$  and  $\hat{\mathbf{K}}_\beta^{(5)}$ , will not be transformed. This is because the physical coordinates of the interface boundary  $\Omega_\beta$  will be used to assemble the reduced matrices for the target and residual parts. This will be explained in the following section.

The reduction procedure for the residual part  $\Omega_A$  is very similar to that of the target part  $\Omega_B$  described above. The transformation matrix for the 1<sup>st</sup> substructure of the residual part  $\Omega_A$  is defined by

$$\mathbf{T}_1^A = \begin{bmatrix} \Phi_1^d & \mathbf{0} & \Psi_{1,3} & \mathbf{0} & \Psi_{1,5} & \Psi_{1,\Gamma} \\ & \mathbf{I}_2 & \mathbf{0} & \mathbf{0} & \mathbf{0} & \mathbf{0} \\ & & \mathbf{I}_3 & \mathbf{0} & \mathbf{0} & \mathbf{0} \\ & & & \mathbf{I}_4 & \mathbf{0} & \mathbf{0} \\ \mathbf{0} & & & & \mathbf{I}_5 & \mathbf{0} \\ & & & & \mathbf{0} & \mathbf{I}_\alpha \end{bmatrix} \quad (29)$$

where the transformation matrix  $\mathbf{T}_1^A$  is an upper triangular matrix, unlike the transformation matrix  $\mathbf{T}_1^B$  in Eq. (15).

Thus, after the sequential transformation procedures with  $\mathbf{T}_2^A$ ,  $\mathbf{T}_3^A$ ,  $\mathbf{T}_4^A$ , and  $\mathbf{T}_5^A$ , the mass and stiffness matrices for the residual part,  $\mathbf{M}_A$  and  $\mathbf{K}_A$ , in Eq. (11) are reduced as follows

$$\bar{\mathbf{M}}_A = \begin{bmatrix} \mathbf{I}_1^d & \mathbf{0} & \bar{\mathbf{M}}_{1,3} & \mathbf{0} & \bar{\mathbf{M}}_{1,5} & \hat{\mathbf{M}}_{1,\Gamma}^{(5)} \\ & \mathbf{I}_2^d & \bar{\mathbf{M}}_{2,3} & \mathbf{0} & \bar{\mathbf{M}}_{2,5} & \hat{\mathbf{M}}_{2,\Gamma}^{(5)} \\ & & \mathbf{I}_3^d & \mathbf{0} & \bar{\mathbf{M}}_{3,5} & \hat{\mathbf{M}}_{3,\Gamma}^{(5)} \\ & & & \mathbf{I}_4^d & \bar{\mathbf{M}}_{4,5} & \hat{\mathbf{M}}_{4,\Gamma}^{(5)} \\ \text{sym.} & & & & \mathbf{I}_5^d & \hat{\mathbf{M}}_{5,\Gamma}^{(5)} \\ & & & & & \hat{\mathbf{M}}_\alpha^{(5)} \end{bmatrix} \quad (30)$$

$$\bar{\mathbf{K}}_A = \begin{bmatrix} \Lambda_1^d & \mathbf{0} & \mathbf{0} & \mathbf{0} & \mathbf{0} & \mathbf{0} \\ & \Lambda_2^d & \mathbf{0} & \mathbf{0} & \mathbf{0} & \mathbf{0} \\ & & \Lambda_3^d & \mathbf{0} & \mathbf{0} & \mathbf{0} \\ & & & \Lambda_4^d & \mathbf{0} & \mathbf{0} \\ \text{sym.} & & & & \Lambda_5^d & \mathbf{0} \\ & & & & & \hat{\mathbf{K}}_\alpha^{(5)} \end{bmatrix}$$

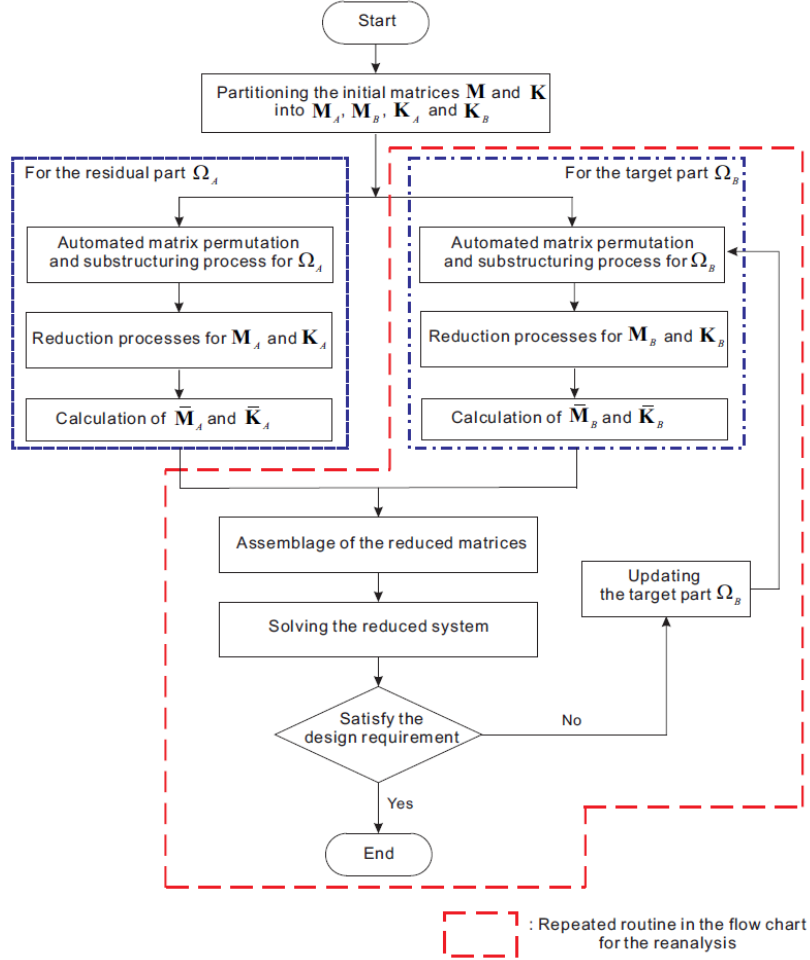


Fig. 4 Algorithm flow chart of the proposed structural modal reanalysis method

where  $\bar{\mathbf{M}}_A$  and  $\bar{\mathbf{K}}_A$  are the completely transformed reduced mass and stiffness matrices for the residual part  $\Omega_A$ . The substructural matrix computations for the residual part  $\Omega_A$  are almost same as that of the target part  $\Omega_B$ , except for conducting the transformation in order. The substructural computation strategy for the reduction has already been well-described by Kaplan (2001).

### 3.4 Assemblage of the reduced matrices and solving the reduced system

From Eq. (27) and Eq. (30), the reduced matrices  $\bar{\mathbf{M}}_A$ ,  $\bar{\mathbf{M}}_B$ ,  $\bar{\mathbf{K}}_A$ , and  $\bar{\mathbf{K}}_B$  are simply rewritten as

$$\bar{\mathbf{M}}_A = \begin{bmatrix} \bar{\mathbf{M}}_a & \hat{\mathbf{M}}_{a,\Gamma} \\ \hat{\mathbf{M}}_{a,\Gamma}^T & \hat{\mathbf{M}}_\alpha^{(5)} \end{bmatrix}, \quad \bar{\mathbf{M}}_B = \begin{bmatrix} \hat{\mathbf{M}}_\beta^{(5)} & \hat{\mathbf{M}}_{\Gamma,b} \\ \hat{\mathbf{M}}_{\Gamma,b}^T & \bar{\mathbf{M}}_b \end{bmatrix} \quad (31)$$

$$\bar{\mathbf{K}}_A = \begin{bmatrix} \Lambda_a^d & \mathbf{0} \\ \mathbf{0} & \hat{\mathbf{K}}_\alpha^{(5)} \end{bmatrix}, \quad \bar{\mathbf{K}}_B = \begin{bmatrix} \hat{\mathbf{K}}_\beta^{(5)} & \mathbf{0} \\ \mathbf{0} & \Lambda_b^d \end{bmatrix}$$

where  $\bar{\mathbf{M}}_A$  and  $\bar{\mathbf{K}}_A$  are  $\bar{N}_A \times \bar{N}_A$  matrices, and  $\bar{\mathbf{M}}_B$  and  $\bar{\mathbf{K}}_B$  are  $\bar{N}_B \times \bar{N}_B$  matrices. Here,  $\bar{N}_A$  and  $\bar{N}_B$

are the size of the reduced models corresponding to the residual and target parts, respectively.

Then, conducting the assemblage of the reduced matrices in Eq. (31), the final reduced mass and stiffness matrices in the proposed method are obtained as follows

$$\bar{\mathbf{M}} = \begin{bmatrix} \bar{\mathbf{M}}_a & \hat{\mathbf{M}}_{a,\Gamma} & \mathbf{0} \\ \hat{\mathbf{M}}_{a,\Gamma}^T & \hat{\mathbf{M}}_\Gamma^{(5)} & \hat{\mathbf{M}}_{\Gamma,b} \\ \mathbf{0} & \hat{\mathbf{M}}_{\Gamma,b}^T & \bar{\mathbf{M}}_b \end{bmatrix}, \quad \bar{\mathbf{K}} = \begin{bmatrix} \Lambda_a^d & \mathbf{0} & \mathbf{0} \\ \mathbf{0} & \hat{\mathbf{K}}_\Gamma^{(5)} & \mathbf{0} \\ \mathbf{0} & \mathbf{0} & \Lambda_b^d \end{bmatrix}, \quad (32)$$

$$\text{with } \hat{\mathbf{M}}_\Gamma^{(5)} = \hat{\mathbf{M}}_\alpha^{(5)} + \hat{\mathbf{M}}_\beta^{(5)}, \quad \hat{\mathbf{K}}_\Gamma^{(5)} = \hat{\mathbf{K}}_\alpha^{(5)} + \hat{\mathbf{K}}_\beta^{(5)}$$

in which  $\bar{\mathbf{M}}$  and  $\bar{\mathbf{K}}$  are  $\bar{N} \times \bar{N}$  matrices ( $\bar{N} = \bar{N}_A + \bar{N}_B - N_\Gamma$ , where  $N_\Gamma$  is the size of the interface boundary  $\Omega_\Gamma$ ).

The eigenvalues and eigenvectors are then approximated from the following reduced eigenvalue problem

$$\bar{\mathbf{K}} \bar{\boldsymbol{\phi}}_i = \bar{\lambda}_i \bar{\mathbf{M}} \bar{\boldsymbol{\phi}}_i \quad \text{for } i = 1, 2, \dots, \bar{N} \quad (33)$$

where  $\bar{\lambda}_i$  and  $\bar{\boldsymbol{\phi}}_i$  are the approximated eigenvalues and eigenvectors, respectively.

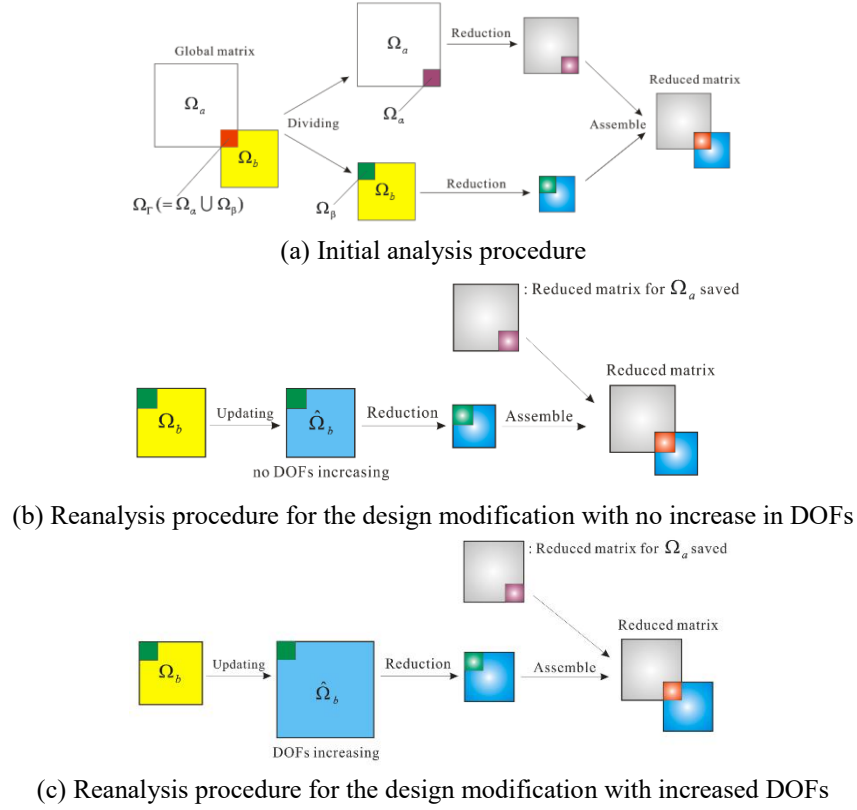


Fig. 5 Global matrix dividing, reduction, and assemblage schematic of the proposed method

To compute the approximated global eigenvectors, a transformation matrix corresponding to the reduced matrices in Eq. (32) is computed. The whole transformation matrices for the residual and target parts are defined by

$$\mathbf{T}_A = \mathbf{T}_1^A \mathbf{T}_2^A \cdots \mathbf{T}_5^A = \prod_{i=1}^5 \mathbf{T}_i^A, \quad \mathbf{T}_B = \mathbf{T}_1^B \mathbf{T}_2^B \cdots \mathbf{T}_5^B = \prod_{i=1}^5 \mathbf{T}_i^B. \quad (34)$$

The substructural matrix computing forms for  $\mathbf{T}_A$  and  $\mathbf{T}_B$  are represented as

$$\mathbf{T}_A = \begin{bmatrix} \Phi_1^d & \mathbf{0} & \bar{\Psi}_{1,3} & \mathbf{0} & \bar{\Psi}_{1,5} & \hat{\Psi}_{1,\Gamma} \\ & \Phi_2^d & \bar{\Psi}_{2,3} & \mathbf{0} & \bar{\Psi}_{2,5} & \hat{\Psi}_{2,\Gamma} \\ & & \Phi_3^d & \mathbf{0} & \bar{\Psi}_{3,5} & \hat{\Psi}_{3,\Gamma} \\ & & & \Phi_4^d & \bar{\Psi}_{4,5} & \hat{\Psi}_{4,\Gamma} \\ \mathbf{0} & & & & \Phi_5^d & \hat{\Psi}_{5,\Gamma} \\ \hline & \mathbf{0} & & & & \mathbf{I}_\alpha \end{bmatrix} \quad (35)$$

$$\mathbf{T}_B = \begin{bmatrix} \mathbf{I}_\beta & & & \mathbf{0} \\ \hat{\Psi}_{5,\Gamma} & \Phi_5^d & & & \\ \hat{\Psi}_{4,\Gamma} & \bar{\Psi}_{4,5} & \Phi_4^d & & \mathbf{0} \\ \hat{\Psi}_{3,\Gamma} & \bar{\Psi}_{3,5} & \mathbf{0} & \Phi_3^d & \\ \hat{\Psi}_{2,\Gamma} & \bar{\Psi}_{2,5} & \mathbf{0} & \bar{\Psi}_{2,3} & \Phi_2^d \\ \hat{\Psi}_{1,\Gamma} & \bar{\Psi}_{1,5} & \mathbf{0} & \bar{\Psi}_{1,3} & \mathbf{0} & \Phi_1^d \end{bmatrix}$$

$$\hat{\Psi}_{i,j} = \Psi_{i,j} + \sum_{\substack{k \in A_i \cap C_j \\ i \in C_j}} \hat{\Psi}_{i,k} \Psi_{k,j} \quad \text{for } k \in A_i \cap C_j \text{ and } i \in C_j \quad (36a)$$

$$\bar{\Psi}_{i,j} = \hat{\Psi}_{i,j} \Phi_j^d \quad \text{for } i \in C_j. \quad (36b)$$

Note that, although the same substructural matrix notations are used in  $\mathbf{T}_A$  and  $\mathbf{T}_B$ , the matrices  $\Phi_i^d$ ,  $\bar{\Psi}_{i,j}$ , and  $\hat{\Psi}_{i,j}$  in  $\mathbf{T}_A$  are different from the matrices  $\Phi_i^d$ ,  $\bar{\Psi}_{i,j}$ , and  $\hat{\Psi}_{i,j}$  in  $\mathbf{T}_B$ .

The transformation matrices in Eq. (35) can simply be rewritten in the following partitioned matrix form

$$\mathbf{T}_A = \begin{bmatrix} \mathbf{T}_a & \mathbf{T}_c^r \\ \mathbf{0} & \mathbf{I}_\alpha \end{bmatrix}, \quad \mathbf{T}_B = \begin{bmatrix} \mathbf{I}_\beta & \mathbf{0} \\ \mathbf{T}_c^t & \mathbf{T}_b \end{bmatrix} \quad (37)$$

and thus, the assembled transformation matrix used to compute the approximated global eigenvectors is obtained as

$$\mathbf{T} = \begin{bmatrix} \mathbf{T}_a & \mathbf{T}_c^r & \mathbf{0} \\ \mathbf{0} & \mathbf{I}_\Gamma & \mathbf{0} \\ \mathbf{0} & \mathbf{T}_c^t & \mathbf{T}_b \end{bmatrix}. \quad (38)$$

Finally, the approximated global eigenvectors of the proposed method is calculated as follows

$$(\bar{\Phi}_g)_i = \mathbf{T} \bar{\Phi}_i \quad \text{for } i = 1, 2, \dots, \bar{N}. \quad (39)$$

Calculation of the reduced matrices  $\bar{\mathbf{M}}_A$  and  $\bar{\mathbf{K}}_A$ , and the transformation matrix  $\mathbf{T}_A$ , which correspond to the

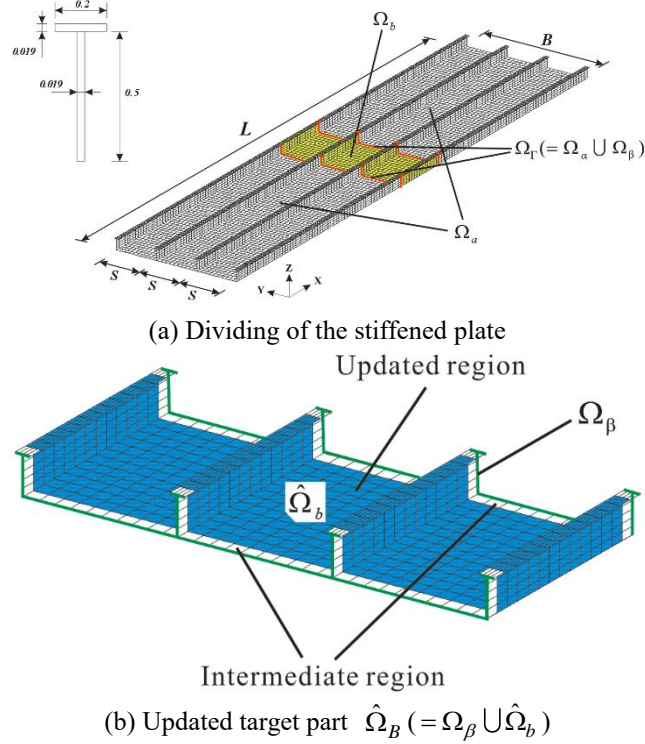


Fig. 6 Stiffened plate problem

residual part  $\Omega_A$ , require relatively large computation times. This is because the residual part  $\Omega_A$  generally has most of the total DOFs.

Fortunately, as mentioned previously, the reduction process for the residual part  $\Omega_A$  is conducted only one time in the initial analysis. When design modifications are required and the structural modal reanalysis is needed several times, we just calculate the reduced matrices  $\bar{\mathbf{M}}_B$  and  $\bar{\mathbf{K}}_B$ , and the transformation matrix  $\mathbf{T}_B$  repeatedly, which correspond to the target part  $\Omega_B$  and contain relatively few DOFs. Because the reduced model for the target part is assembled with that of the residual part already saved, the final reduced model corresponding to the new design can be obtained very quickly. The algorithm flow chart of the proposed structural modal reanalysis method is described in Fig. 4.

Another attractive feature of the proposed method is that it can handle topological modification problems very effectively; however, this induces a change of the number of DOFs (increase or decrease) in FE models. Fig. 5 shows the global matrix dividing, reduction, and assemblage schematic of the proposed method, and Fig. 5(c) shows the reanalysis procedure for the design modification that induces a change of the number of DOFs.

The things mentioned above are the most attractive features of the proposed method, and these are discussed, along with several engineering examples, in the following section.

#### 4. Numerical examples

In this section, to investigate the performance of the proposed method, a stiffened plate, a cargo-hold structure, and a spar structure are tested. These involve from 52662 to 1182162 DOFs. For all the structural problems, the free boundary condition is imposed. The performance of the proposed method is compared to that of reanalysis using the AMLS method (Bennighof and Lehoucq 2004), which is the most efficient substructuring method for solving large FE models. For a fair comparison, the same size of reduced model is considered for the proposed and AMLS methods.

The automated matrix permutation and substructuring is accomplished using METIS (Karypis and Kumar 1998), which is an efficient matrix permutation and substructuring software package.

The numerical code is implemented with MATLAB and a personal computer (Intel core (TM) i7-3770, 3.40 GHz CPU, 32 GB RAM) is used for computation.

To verify the reliability of the proposed method, the approximated eigenvalues ( $\bar{\lambda}_i$ ) and eigenvectors ( $\bar{\varphi}_g$ ) obtained from the reduced model are compared with its exact values obtained from the global FE model. For this, the following relative eigenvalue error and the modal assurance criterion (MAC) (Pastor *et al.* 2012) are used.

$$\xi_i = \frac{|\bar{\lambda}_i - \lambda_i|}{\lambda_i} \quad (40a)$$

$$\text{MAC}(i, j) = \frac{|(\bar{\varphi}_g)_i^T (\bar{\varphi}_g)_j|^2}{((\bar{\varphi}_g)_i^T (\bar{\varphi}_g)_i)((\bar{\varphi}_g)_j^T (\bar{\varphi}_g)_j)} \quad (40b)$$

for  $i, j = 1, 2, \dots, \bar{N}$

Table 1 Exact eigenvalue  $\lambda_i$  corresponding to the 1<sup>st</sup>–10<sup>th</sup> modes of the initial, 1<sup>st</sup> modified, and 2<sup>nd</sup> modified stiffened plates

Mode number	Exact eigenvalue $\lambda_i$		
	Initial	1 <sup>st</sup> modified	2 <sup>nd</sup> modified
1	9.78E+00	1.55E+01	2.94E+01
2	2.73E+02	3.30E+02	3.79E+02
3	3.08E+02	3.95E+02	6.08E+02
4	7.99E+02	8.22E+02	8.44E+02
5	9.90E+02	1.01E+03	9.85E+02
6	1.90E+03	2.00E+03	2.09E+03
7	1.96E+03	2.24E+03	2.57E+03
8	2.07E+03	2.40E+03	2.65E+03
9	3.63E+03	4.94E+03	5.26E+03
10	5.18E+03	5.24E+03	5.53E+03

Table 2 Relative eigenvalue errors and diagonal MAC values corresponding to the 1<sup>st</sup>–10<sup>th</sup> modes for the stiffened plate problem, derived from the 1<sup>st</sup> and 2<sup>nd</sup> structural modal reanalysis using the proposed method

Mode number	Relative eigenvalue errors $\xi_i$		Diagonal MAC values	
	1 <sup>st</sup>	2 <sup>nd</sup>	1 <sup>st</sup>	2 <sup>nd</sup>
	reanalysis	reanalysis	reanalysis	reanalysis
1	1.41E-06	2.65E-06	1.00	1.00
2	2.42E-05	2.76E-05	1.00	1.00
3	2.69E-05	3.89E-05	1.00	1.00
4	8.97E-05	7.48E-05	1.00	1.00
5	4.18E-05	3.83E-05	1.00	1.00
6	1.75E-04	1.86E-04	1.00	1.00
7	9.70E-05	1.06E-04	1.00	1.00
8	1.86E-04	2.18E-04	1.00	1.00
9	2.91E-04	3.19E-03	1.00	1.00
10	3.28E-03	4.91E-04	0.99	1.00

Table 3 Computation times for the structural modal reanalysis in the stiffened plate problem

Methods	Computation times (sec)		
	Initial	1 <sup>st</sup> reanalysis	2 <sup>nd</sup> reanalysis
Global	376.78	375.69	376.26
AMLS	35.46	34.92	33.96
Proposed	35.60	7.31	6.57

in which  $\xi_i$  denotes the relative eigenvalue error, and  $\lambda_i$  and  $(\boldsymbol{\varphi}_g)_i$  denote the exact global eigenvalue and eigenvector for the  $i^{\text{th}}$  mode.

To calculate the exact eigenpairs,  $\lambda_i$  and  $\boldsymbol{\varphi}_g$ , the ‘eigs’ function in MATLAB is used, which is usually employed for solving large scale eigenvalue problems with sparse matrices. It gives a subset of eigenpairs. The MAC values indicate consistency between eigenvectors  $\boldsymbol{\varphi}_g$  and

$\bar{\boldsymbol{\varphi}}_g$  by a value from zero to unity. If the MAC value is near unity, the eigenvectors,  $\boldsymbol{\varphi}_g$  and  $\bar{\boldsymbol{\varphi}}_g$ , are considered consistent.

#### 4.1 Stiffened plate problem

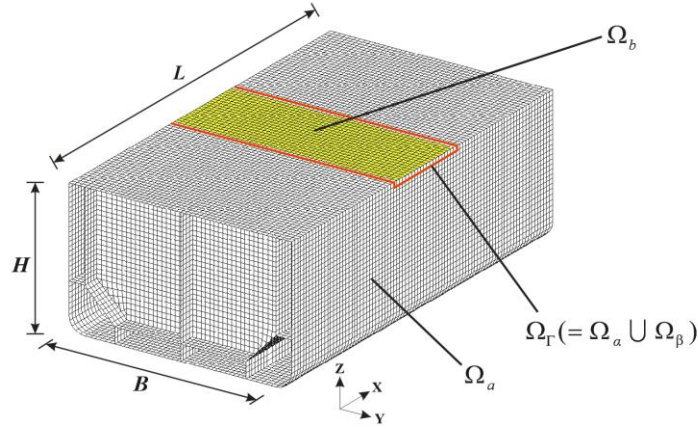
As shown in Fig. 6, a stiffened plate (a primary component of ships and offshore structures), is considered. Its length  $L$  and breadth  $B$  are 26 and 6 m, respectively, and the stiffener spacing  $S$  is 2.0 m. The stiffener  $s$  composed of a flange of breadth 0.2 m and a vertical web of height 0.5 m. The thickness  $h$  is 0.019 m. The stiffened plate is modeled with 8580 shell finite elements, and its number of DOFs is 52662.

If a design modification (in this case, a change of thickness) is required at the center of the stiffened plate, based on Fig. 1, the stiffened plate is divided into  $\Omega_a$ ,  $\Omega_b$ , and  $\Omega_\Gamma$  ( $=\Omega_a \cup \Omega_b$ ), as shown in Fig. 6(a). The target part  $\Omega_B$  ( $=\Omega_\beta \cup \Omega_b$ ) to be modified is highlighted in yellow. In this problem, the thickness change at the target part is considered two times (0.050 and 0.075 m, respectively). The number of DOFs of the target part  $\Omega_B$  is 6030, and Fig. 6(b) shows the updated target part  $\hat{\Omega}_B$  ( $=\Omega_\beta \cup \hat{\Omega}_b$ ).

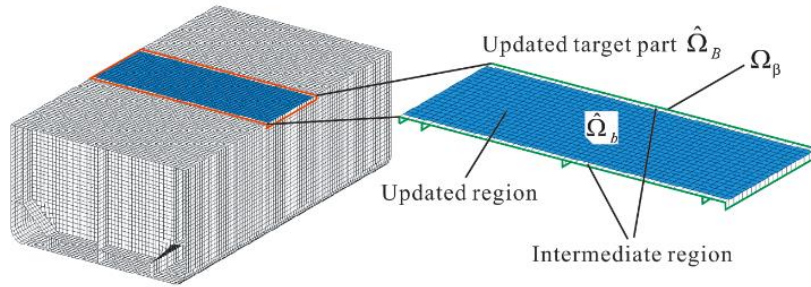
Using METIS, the mass and stiffness matrices for the residual part  $\Omega_A$  are partitioned into 255 substructures and the interface boundary  $\Omega_\alpha$ , and the substructural leveling graph is constructed with eight levels. For the target part  $\Omega_B$ , the mass and stiffness matrices are partitioned into 63 substructures and the interface boundary  $\Omega_\beta$  with six substructural levels. The size of the reduced matrix constructed using the proposed method is  $\bar{N} = 3474$  ( $\bar{N} = \bar{N}_A + \bar{N}_B - N_\Gamma$ , where  $\bar{N}_A = 3206$ ,  $\bar{N}_B = 1072$ , and  $N_\Gamma = 804$ ) for the two cases considered.

Table 1 demonstrates the exact eigenvalues  $\lambda_i$  for the initial, 1<sup>st</sup> modified, and 2<sup>nd</sup> modified stiffened plates, which correspond to the 1<sup>st</sup>–10<sup>th</sup> modes. Table 2 represents the relative eigenvalue errors and diagonal MAC values, which are derived from the 1<sup>st</sup> and 2<sup>nd</sup> structural modal reanalysis using the proposed method.

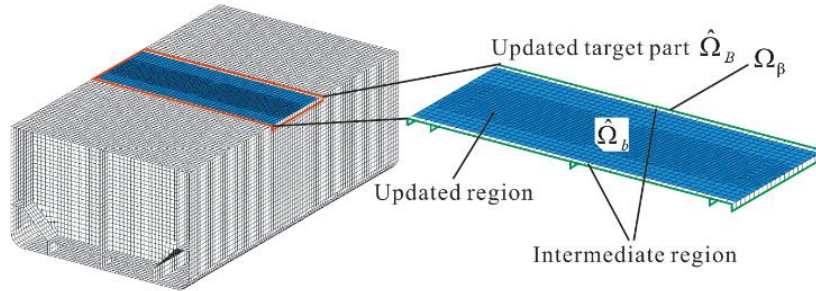
Table 3 shows the computation times for the stiffened plate problem. The proposed method requires 7.31 and 6.57 seconds to conduct the 1<sup>st</sup> and 2<sup>nd</sup> structural modal reanalysis, while the original AMLS method requires 34.92 and 33.96 seconds. Note that, the computation times for the 1<sup>st</sup> reanalysis of the proposed method is dramatically reduced compared to that of the initial analysis. This is because the reduced model for the residual part  $\Omega_A$ , which is already obtained in the initial analysis, is reused, and only the reduction process of the updated target part  $\hat{\Omega}_B$  is conducted. This is the most efficient aspect of the proposed method for reducing the computation time for structural modal reanalysis. From these results, we confirm the excellent computational efficiency of the proposed method.



(a) Dividing of the cargo-hold structure



(b) The 1<sup>st</sup> modification (thickness)



(c) The 2<sup>nd</sup> modification (re-mesh)

Fig. 7 Cargo-hold structure problem

Table 4 Exact eigenvalue  $\lambda_i$  corresponding to the 1<sup>st</sup>-10<sup>th</sup> modes of the initial, 1<sup>st</sup> modified, and 2<sup>nd</sup> modified cargo-hold structures

Mode number	Exact eigenvalue $\lambda_i$		
	Initial	1 <sup>st</sup> modified	2 <sup>nd</sup> modified
1	2.42E+00	2.99E+00	2.99E+00
2	3.30E+00	3.60E+00	3.60E+00
3	4.99E+00	5.32E+00	5.32E+00
4	5.10E+00	6.70E+00	6.70E+00
5	6.14E+00	7.25E+00	7.25E+00
6	6.64E+00	8.22E+00	8.22E+00
7	7.97E+00	8.31E+00	8.31E+00
8	7.99E+00	8.44E+00	8.44E+00
9	8.03E+00	8.56E+00	8.56E+00
10	8.09E+00	8.93E+00	8.93E+00

Table 5 Relative eigenvalue errors and diagonal MAC values corresponding to the 1<sup>st</sup>-10<sup>th</sup> modes for the cargo-hold structure problem, derived from the 1<sup>st</sup> and 2<sup>nd</sup> structural modal reanalysis using the proposed method

Mode number	Relative eigenvalue errors		Diagonal MAC values	
	$\xi_i$		1 <sup>st</sup> reanalysis	2 <sup>nd</sup> reanalysis
	1 <sup>st</sup> reanalysis	2 <sup>nd</sup> reanalysis		
1	2.90E-05	2.87E-05	1.00	1.00
2	3.24E-05	3.24E-05	1.00	1.00
3	5.64E-05	5.63E-05	1.00	1.00
4	7.15E-05	6.80E-05	1.00	1.00
5	8.91E-05	8.85E-05	1.00	1.00
6	5.80E-05	5.80E-05	1.00	1.00
7	1.52E-04	1.52E-04	1.00	1.00
8	1.52E-04	1.51E-04	1.00	1.00
9	2.88E-04	2.88E-04	1.00	1.00
10	1.32E-04	1.30E-04	1.00	1.00

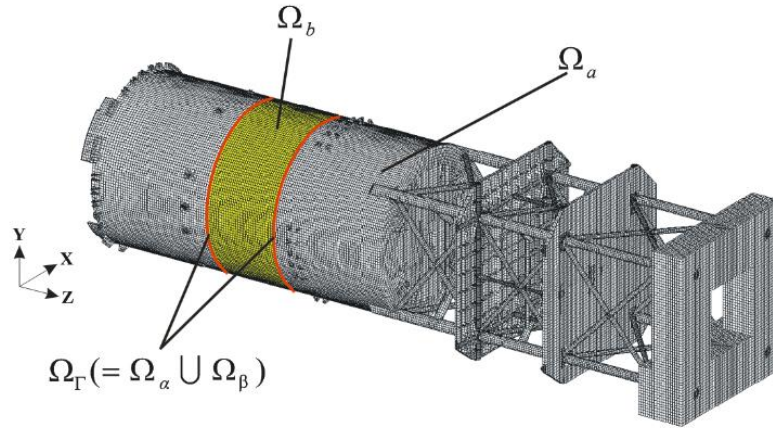


Fig. 8 Spar structure problem

Table 6 Computation times for the structural modal reanalysis in the cargo-hold structure problem

Methods	Computation times (sec)		
	Initial	1 <sup>st</sup> reanalysis	2 <sup>nd</sup> reanalysis
Global	857.27	861.87	905.57
AMLS	332.30	329.71	334.48
Proposed	346.53	34.18	43.87

Table 7 Relative eigenvalue errors and diagonal MAC values corresponding to the 1<sup>st</sup>–15<sup>th</sup> modes for the spar structure problem, derived from the 1<sup>st</sup> and 2<sup>nd</sup> structural modal reanalysis using the proposed method

Mode number	Relative eigenvalue errors		Diagonal MAC values	
	$\xi_i$			
	1 <sup>st</sup> reanalysis (thickness)	2 <sup>nd</sup> reanalysis (topology)	1 <sup>st</sup> reanalysis (thickness)	2 <sup>nd</sup> reanalysis (topology)
1	6.06E-04	5.59E-04	1.00	1.00
2	1.91E-03	1.96E-03	1.00	1.00
3	1.46E-03	1.49E-03	1.00	1.00
4	5.37E-04	6.91E-03	1.00	1.00
5	3.14E-04	1.12E-03	1.00	1.00
6	3.86E-04	3.13E-04	1.00	1.00
7	1.36E-02	3.89E-04	1.00	1.00
8	6.50E-03	8.78E-04	1.00	1.00
9	8.72E-04	5.59E-03	1.00	1.00
10	5.59E-03	9.14E-03	1.00	1.00
11	1.21E-02	7.29E-03	0.88	1.00
12	1.35E-02	8.98E-03	0.88	1.00
13	7.89E-03	7.21E-02	1.00	1.00
14	9.39E-03	1.73E-01	1.00	1.00
15	8.51E-03	1.67E-01	1.00	1.00

#### 4.2 Cargo-hold structure problem

Here, a cargo-hold structure of an oil carrier is considered, as shown in Fig. 7. The height  $H$ , breadth  $B$ , length  $L$ , and thickness  $t$  are 30.0, 50.0, 87.0, and 0.012 m, respectively. For finite element modeling, 26761 shell

elements and 26228 nodes are used, and the number of total DOFs is 157368.

As shown in Fig. 7(a), the design modifications are imposed at the center of the deck plate. Then, the cargo-hold structure is divided into  $\Omega_a$ ,  $\Omega_b$ , and  $\Omega_\Gamma$  ( $= \Omega_\alpha \cup \Omega_\beta$ ). The target part  $\Omega_B$  ( $= \Omega_\beta \cup \Omega_b$ ) is highlighted in yellow, and the number of DOFs in the target part  $\Omega_B$  is 7128.

Two design modifications are considered in this problem. One is to change the thickness of the target part to 0.025 m, and the other is to change the mesh of the target part to very fine elements, as shown in Fig. 7(b) and 7(c).

Here, the fine mesh increases the number of DOFs in the target part by 1280. In this problem, structural modal reanalysis is performed for each of the two modifications considered.

From the automated matrix permutation and substructuring process, 1023 substructures and the interface boundary  $\Omega_\alpha$  are defined with the substructural leveling graph of ten levels for the residual part  $\Omega_A$ . For the target part  $\Omega_B$ , 63 substructures and the interface boundary  $\Omega_\beta$  are defined with the substructural leveling graph with six levels. The sizes of the reduced matrices constructed by the proposed method are  $\bar{N} = 9252$  ( $\bar{N}_A = 8950$ ,  $\bar{N}_B = 1550$ ), and  $N_\Gamma = 1248$ ) and  $\bar{N} = 9656$  ( $\bar{N}_A = 8950$ ,  $\bar{N}_B = 1954$ , and  $N_\Gamma = 1248$ ) for the two cases considered.

The exact eigenvalue  $\lambda_i$  for the initial, 1<sup>st</sup> modified, and 2<sup>nd</sup> modified cargo-hold structures are listed in Table 4, while Table 5 presents the relative eigenvalue errors and diagonal MAC values for the modified cargo-hold structures.

Table 6 shows the computation times of the structural modal reanalysis. For the initial model, and the 1<sup>st</sup> and 2<sup>nd</sup> modified models, the structural modal analysis handling the global FE model requires 857.27, 861.87, and 905.57 seconds, respectively. Here, computation times corresponding to the global FE model represent the time to calculate a subset of eigenpairs, which is about 0.05% (780 eigenpairs) of the total DOFs.

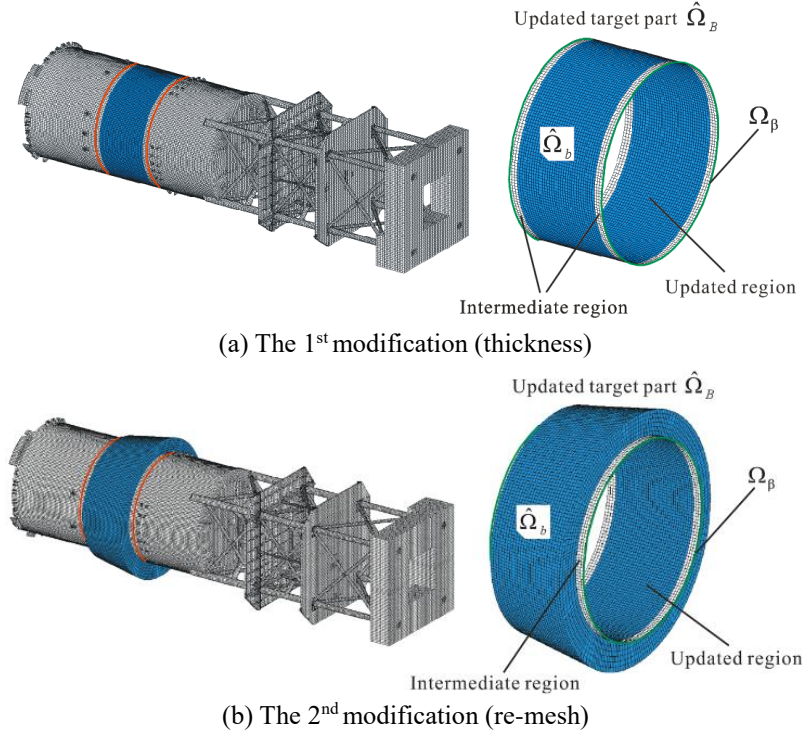
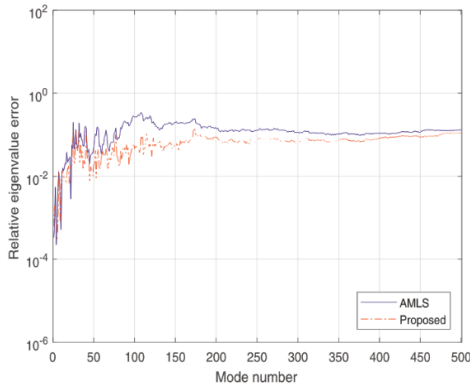
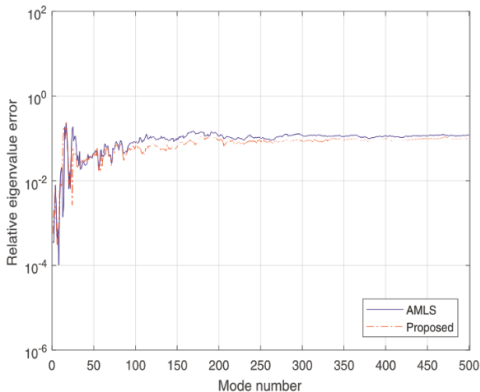


Fig. 9 Design modifications for the spar structure problem



(a) Reanalysis for the 1<sup>st</sup> modification (thickness)



(b) Reanalysis for the 2<sup>nd</sup> modification (topological)

Fig. 10 Relative eigenvalue errors for the spar structure problem

The original AMLS method requires 332.30, 329.71, and 334.48 seconds, respectively, and the proposed method

requires 346.53, 34.18, and 43.87 seconds, respectively.

For the 2<sup>nd</sup> reanalysis of the re-mesh case, the proposed method is 7.62 and 20.64 times faster than reanalysis using the original AMLS method and global FE model, respectively.

As mentioned previously, this is because the residual part  $\Omega_A$ , including most of the total DOFs, is reduced in the initial analysis, and this reduced model is reused repeatedly in each reanalysis.

### 4.3 Spar structure problem

A spar structure is considered as shown in Fig. 8. For finite element modeling, 203565 shell elements and 189334 nodes are used, and the number of total DOFs is 1136004.

For this spar structure problem, as shown in Fig. 9, structural modal reanalysis was conducted after considering thickness and again after topological modifications.

The number of DOFs in the target part  $\Omega_B$  is 51168. For the thickness modification case, the thickness of the target part is changed from 0.030 to 0.050 m, and for the topological modification case, 0.050 m of thickness is substituted and the number of DOFs in the target is increased to 97326. Structural modal reanalysis is performed for each of the two modifications considered.

In this spar structure problem, 2047 substructures and 11 substructural levels are used for the residual part  $\Omega_A$ , and 255 substructures and 8 substructural levels are used for the target part  $\Omega_B$ .

The sizes of the reduced matrices obtained by the proposed method are  $\bar{N} = 20595$  ( $\bar{N}_A = 19795$ ,  $\bar{N}_B = 3296$ , and  $N_T = 2496$ ) and  $\bar{N} = 21320$  (

Table 8 Specific computation times for the structural modal reanalysis in the spar structure problem

Methods	Items	Computation times [sec]		
		Initial	1 <sup>st</sup> reanalysis	2 <sup>nd</sup> reanalysis
Global	Generalized eigenvalue problem	8658.75	8663.24	9147.02
	Transformation procedure	5263.35	5274.53	5286.81
AMLS	Reduced eigenvalue problem	138.40	133.46	147.75
	Total	5401.75	5407.99	5434.56
Proposed	Definition of the residual and target parts, $\Omega_A$ and $\Omega_B$	4.03	-	-
	Automated matrix permutation and substructuring process for $\Omega_A$	8.23	-	-
	Reduction process for $\Omega_A$	4874.32	-	-
	Automated matrix permutation and substructuring process for $\Omega_B$	4.21	4.16	4.57
	Reduction process for $\Omega_B$	86.79	90.70	221.01
	Assemblage process of the reduced matrices	4.51	4.45	4.80
	Reduced eigenvalue problem	348.05	343.42	359.48
	Total	5330.14	442.73	589.86

$\bar{N}_A = 19795$ ,  $\bar{N}_B = 4021$ , and  $N_T = 2496$ ) respectively, for the cases considered.

Fig. 10 shows the relative eigenvalue errors, derived from the 1<sup>st</sup> and 2<sup>nd</sup> structural modal reanalysis for the spar structure problem. Table 7 lists the relative eigenvalue errors and diagonal MAC values corresponding to the 1<sup>st</sup>-15<sup>th</sup> modes.

Table 8 shows the specific computation times for the structural modal reanalysis in the spar structure problem. For the global FE model, the initial analysis, and 1<sup>st</sup> and 2<sup>nd</sup> reanalysis require 8658.75, 8663.24, and 9147.02 seconds, respectively, to calculate 500 global eigenpairs. For the AMLS method, 5401.75, 5407.99, and 5434.56 seconds are required, respectively. In contrast, the proposed method requires 5330.14 seconds for the initial analysis, and only 442.73 and 589.86 seconds for reanalysis.

From these results, we can clearly see that the proposed structural modal reanalysis method shows excellent computational efficiency and reanalysis ability.

## 5. Conclusions

In this study, to conduct structural modal analysis efficiently for large FE models requiring frequent design modification, a novel structural modal reanalysis method was proposed.

- A global FE model was divided into a residual part not to be modified and a target part to be modified.

- An automated matrix permutation and substructuring algorithm was employed independently for these two parts, and each reduced model was constructed using the AMLS method.

- The reduced model for the residual part was saved in the initial analysis, and the reduced model for the target part was calculated repeatedly according to the design modifications considered, affecting such as thickness, mesh, and topological changes.

- The final reduced model corresponding to the new design was easily and quickly constructed through a simple

process for assemblage of the reduced model of the residual part already saved and that of the target part repeatedly calculated. This is the key feature of the proposed method for reducing the computation time dramatically for structural modal reanalysis.

- In this paper, the formulation was derived in detail, and the excellent computational efficiency and reanalysis ability of the proposed method were well demonstrated through various practical engineering problems.

In future work, it would be valuable to employ a parametrization scheme (Hong *et al.* 2013) for the proposed method for efficient design optimization. It would also be valuable to expand the proposed method to a free-interface substructuring technique (Kim *et al.* 2017), in which each substructure is linked with the Lagrange multiplier.

## Acknowledgments

This work was supported by the Korea Maritime and Ocean University Research Fund.

## References

- Benfield, W.A. and Hrudá, R.F. (1971), "Vibration analysis of structures by component mode substitution", *AIAA J.*, **9**, 1255-1261.
- Bennighof, J.K. and Lehoucq, R.B. (2004), "An automated multilevel substructuring method for eigenspace computation in linear elastodynamics", *SIAM J. Sci. Comput.*, **25**(6), 2084-2106.
- Boo, S.H. and Lee, P.S. (2017), "A dynamic condensation method using algebraic substructuring", *Int. J. Numer. Meth. Eng.*, **109**(12), 1701-1720.
- Boo, S.H. and Lee, P.S. (2017), "An iterative algebraic dynamic condensation method and its performance", *Comput. Struct.*, **182**, 419-429.
- Boo, S.H. and Oh, M.H. (2017) "Automated static condensation method for local analysis of large finite element models", *Struct. Eng. Mech.*, **61**(6), 807-816.

- Boo, S.H., Kim, J.H. and Lee, P.S. (2018), "Towards improving the enhanced Craig-Bampton method", *Comput. Struct.*, **196**, 63-75.
- Chen, S. and Rong, F. (2002), "A new method of structural modal reanalysis for topological modifications", *Fin. Elem. Analy. Des.*, **38**(11), 1015-1028.
- Craig, R.R. and Bampton, M.C.C. (1968), "Coupling of substructures for dynamic analysis", *AIAA J.*, **6**(7), 1313-1319.
- George, A. (1973), "Nested dissection of a rectangular finite element mesh", *SIAM J. Numer. Analy.*, **10**(2), 345-363.
- Givoli, D., Barbone, P.E. and Patlashenko, I. (2004), "Which are the important modes of a subsystem?", *Int. J. Numer. Meth. Eng.*, **59**(2), 1657-1678.
- Han, J.S. (2014), "Krylov subspace-based model order reduction for Campbell diagram analysis of large-scale rotordynamic systems", *Struct. Eng. Mech.*, **50**(1), 19-36.
- Hendrickson, B and Rothberg, E. (1997), "Effective sparse matrix ordering: Just around the bend", *Proceedings of the 8th SIAM Conference on Parallel Processing for Scientific Computing*, Minnesota, U.S.A., March.
- Hong, S.K., Epureanu, B.I. and Castanier, M.P. (2013), "Next-generation parametric reduced-order models", *Mech. Syst. Sign. Pr.*, **37**(1-2), 403-421.
- Jian-Jun, H., Xiang-Zi, C. and Bin, X. (2015), "Structural modal reanalysis for large, simultaneous and multiple type modifications", *Mech. Syst. Sign. Pr.*, **62**, 207-217.
- Kaplan, M.F. (2001), "Implementation of automated multi-level substructuring for frequency response analysis of structures", Ph.D. Dissertation, University of Texas at Austin, Austin, TX.
- Karypis, G. and Kumar, V. (1998), "METIS v4.0, A software package for partitioning unstructured graphs, partitioning meshes, and computing fill-reducing orderings of sparse matrices", Technical Report, University of Minnesota, Minneapolis, MN, U.S.A.
- Kaveh, A and Fazli, H. (2011), "Approximate eigensolution of locally modified regular structures using a substructuring technique", *Comput. Struct.*, **89**(5-6), 529-537.
- Kim, J.H., Kim, J. and Lee, P.S. (2017), "Improving the accuracy of the dual Craig-Bampton method", *Compt. Struct.*, **191**, 22-32.
- Leung, Y.T. (1979), "An accurate method of dynamic substructuring with simplified computation", *Int. J. Numer. Meth. Eng.*, **14**(8), 1241-1256.
- Papadimiriou, C. and Papadioti, D.C. (2013), "Component mode synthesis technique for finite element model updating", *Comput. Struct.*, **126**, 15-28.
- Pastor, M., Binda, M. and Harčarik T. (2012), "Modal assurance criterion", *Proc. Eng.*, **48**, 543-548.
- Perdahcıođlu, D., Ellenbroek, M., Geijselaers, H. and De Boer, A. (2011), "Updating the Craig-Bampton reduction basis for efficient structural reanalysis", *Int. J. Numer. Meth. Eng.*, **85**(5), 607-624.
- Rubin, S. (1975), "Improved component-mode representation for structural dynamic analysis", *AIAA J.*, **13**(8), 995-1006.
- Soize, C. and Mziou, S. (2003), "Dynamic substructuring in the medium-frequency range", *AIAA J.*, **41**(6), 1113-1118.